



A numerical study of fluid flow and heat transfer in eccentric curved annuli

M.R.H. Nobari*, M.T. Mehrabani

Department of Mechanical Engineering, Amirkabir University of Technology, 424 Hafez Ave., P.O. Box 15875-4413, Tehran, Iran

ARTICLE INFO

Article history:

Received 2 February 2009

Received in revised form

22 June 2009

Accepted 7 July 2009

Available online 29 July 2009

Keywords:

Curved pipe

Eccentric annulus

Incompressible flow

Finite difference

Projection method

ABSTRACT

In this article fluid flow and heat transfer in curved eccentric annuli are studied numerically. A second order finite difference method based on the Projection algorithm is implemented to solve the governing equations including the full Navier–Stokes, the continuity, and the energy equations in a toroidal coordinate system. For convenience a bipolar based toroidal coordinate system is employed to discretize the governing equations in the annulus domain using a uniform staggered grid which is required in finite difference methods. Considering hydrodynamically and thermally fully developed conditions, the effects of different physical parameters such as eccentricity, Dean number, curvature, Prandtl number on the flow field and thermal characteristics at different thermal boundary conditions are investigated in detail. It is also shown that in contrast to straight eccentric annuli, heat transfer rates can be augmented in the eccentric curved annuli comparing with the straight concentric annuli at the large dean numbers.

© 2009 Elsevier Masson SAS. All rights reserved.

1. Introduction

Flow and heat transfer in curved eccentric annuli encounter in many engineering problems such as heat exchangers, lubrication systems, aerospace industries, chemical reactors, and in bio-mechanics such as blood flow in catheterized artery, angiography or arteriography of the blood vessel, etc. Therefore, understanding the detailed physics of the problem will help improve the design of the systems concerned.

The physics of the fluid flow inside the curved pipes are very much complicated due to the presence of curvature generating centrifugal and pressure forces in the curvature direction. In contrast to the centrifugal forces, the pressure forces decrease in the curvature direction as the fluid particles approach center of curvature. Mutual effects of the centrifugal, pressure, inertia and viscous forces provide a very complex flow pattern which has not physically fully understood. A relatively detailed qualitative physical description of the flow in a plain curved pipe has been carried out by Yao and Berger [1]. However, shifting from a plain curved pipe flow to eccentric curved annuli makes the flow pattern more complex owing to the presence of an additional internal curved pipe as well as eccentricity effect. In this case the secondary boundary layers start developing on the walls of both curved pipes

from their outermost point of the curvatures, where the pressure forces are more than the centrifugal ones. On the other hand, in the core region of the two pipe walls, the reverse fluid motion, i.e. from the inner to the outer radii of curvature, occurs resulting from the larger centrifugal and smaller pressure forces. This secondary core flow which starts from the symmetrical plane at the inner radii of the curvature ($\xi = \pi$) develops similar to a jet flow and interacts with the opposite flowing secondary boundary layers forming two pairs of vortices, a weak pair close to the inner pipe and a strong one close to the outer pipe. This phenomenon implies a physical point that in the secondary flows the diffusion of viscous forces occurs more rapidly than the main axial flow owing to the presence of small inertia forces (order of magnitude of secondary inertia forces is about 10^{-1} of the axial one).

Studies on the fluid flow and heat transfer inside an eccentric annulus have been carried out for straight annuli considering either horizontal or vertical cases which include both the fully developed and developing flows. One of the early works is related to Snyder [2] who studied heat transfer in an eccentric annulus under the slug flow assumption by an analytical approach. He considered fully developed condition with the outer pipe as insulated. Laminar forced convection in eccentric annuli has been studied by Cheng and Hwang [3], Trombetta [4], and Susuki et al. [5] using analytical and numerical tools at different thermal boundaries. Manglik and Fang [6] have studied the effect of eccentricity on the heat transfer using different thermal boundary conditions in laminar fully developed conditions. They have indicated that the Nusselt number decreases

* Corresponding author. Tel.: +98 21 64543412; fax: +98 21 66419736.

E-mail address: mrnobari@aut.ac.ir (M.R.H. Nobari).

Nomenclature

a	radius of curvature and the pole of the bipolar coordinate system on the x -axis
c_p	specific heat at constant pressure
D_h	hydraulic diameter, $D_h = 2(r_o - r_i)$
e	eccentricity
E	dimensionless eccentricity, $e/r_o - r_i$
f	average friction factor
f_i	local friction factor on inner wall
f_o	local friction factor on outer wall
h	coordinate scale factor
Gr	Grashof number
h_η	coordinate scale factor in the η direction
h_ξ	coordinate scale factor in the ξ direction
h_φ	coordinate scale factor in the φ direction
k	thermal conductivity
k_{LC}	Dean number, $Re/\lambda^{1/2}$
\vec{n}	unit normal vector
N	radius ratio, r_i/r_o
Nu	average Nusselt number
Nu_ξ	local Nusselt number
p	pressure
Pr	Prandtl number, $Pr = \nu/\alpha$
q''	heat flux
r_i	inner pipe radius
r_o	outer pipe radius

Re	Reynolds number, $Re = w_m D_h / \nu$
t	time
T	temperature
\bar{T}	average temperature
T_m	bulk fluid temperature
u, v, w	velocity components in ξ , η and φ direction, respectively
\mathbf{V}	velocity vector
w_m	mean axial velocity

Greek symbols

α	thermal diffusivity
η	first bipolar coordinate
λ	curvature ratio, $\lambda = a/D_h$
θ	non-dimensional temperature
μ	viscosity of fluid
ν	kinematic viscosity
ξ	second bipolar coordinate
ρ	density of fluid
τ	stress
φ	curvature coordinate

Subscripts

i	inner wall
m	average value
o	outer wall

as the eccentricity increases. Therefore, concentric pipes have better heat transfer rate than the similar straight eccentric annuli. The studies by Feldman et al. [7,8] have investigated developing flow and temperature inside eccentric annular ducts using a finite difference method. They have examined different thermal boundary conditions and shown that both hydrodynamic and thermal entrance lengths increase as the eccentricity increases. A numerical study for steady laminar two-dimensional natural convection in concentric and eccentric horizontal cylindrical annuli has been carried out by Ho et al. [9] who have applied a constant heat flux on the inner wall and a specified isothermal temperature on the outer wall to study the effect of the Prandtl number and the eccentricity on the heat transfer rate. They have shown the heat transfer rate weakly depends on the Prandtl number but primarily depends on the eccentricity. Hirose et al. [10] have conducted numerical analyses and experiments on the natural convection heat transfer in eccentric horizontal annuli between a heated outer tube and a cooled inner tube with different orientations. They have found that the heat transfer changes by eccentricity and oriented angle. Furthermore, an experimental and numerical study have been performed by Naylor et al. [11] on the natural convection heat transfer from a horizontal isothermal inner tube to a surrounding isothermal outer tube. They have discussed how differently eccentricity affects on the heat transfer at different range of Rayleigh numbers. The study by Sathyamurthy et al. [12] has focused on the laminar mixed convection in a vertical eccentric annulus where a finite volume approach has been employed to solve the governing equations. On the other hand, Choudhury and Karki [13] have investigated laminar mixed convection in a horizontal eccentric annulus by a numerical approach to study the eccentricity effect on the heat transfer rate and friction. Also, other works in vertical annuli using finite difference method have been performed to study developing forced convection [14], conjugate natural convection heat transfer [15],

limiting values for free-convection induced flow rates [16], and developing mixed convection [17]. All the works published in the eccentric annuli only involves straight pipes.

Since the aim of this study is fluid flow and heat transfer in eccentric curved annuli, it is necessary to review some of the works done on the curved pipe flows. The first major study on the flow in the curved pipe was made by Dean [18,19] who considered a loosely curved pipe where the flow depends on a single non-dimensional parameter, i.e. the Dean number, $K = 2a/R(w_{\max}a/\nu)^2$, where a is the radius of pipe, R is the radius of curvature, w_{\max} is the maximum axial velocity in the corresponding straight pipe, and ν is the kinematic viscosity. Dean's work is valid for $K \leq 576$. In later works on curved pipes, a variety of Dean numbers have been used by

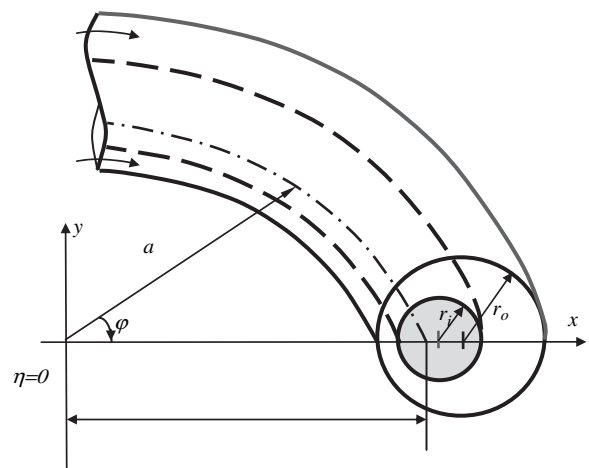


Fig. 1. Geometry of the physical domain.

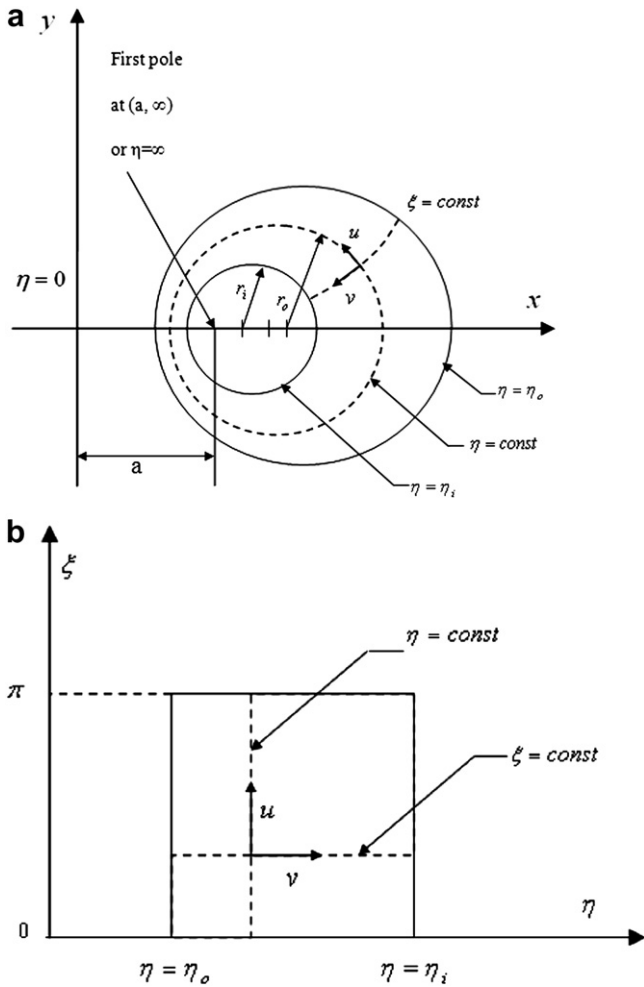


Fig. 2. The geometry in the bipolar coordinate, a: Physical domain, b: Computational domain.

Dean's work becomes 96. They considered intermediate range of Dean numbers ($96 \leq D \leq 600$) using Fourier series method to formulate the problem and solve the resulting equations numerically. Collins and Dennis [21], and Dennis [22] used finite difference method to solve the flow equations in the range of $96 \leq D \leq 5000$. An investigation on developing laminar flow in a curved pipe was made by Soh and Berger [23] using artificial compressibility technique. They found that the curvature ratio has great effect on the intensity of secondary flow and the separation which occurs near the inner wall of curved pipe. Among other similar works on flow in a stationary curved pipe, the works of Pedley [24], Dennis and Ng [25], Ito [26] and Kao [27] can be mentioned. Nobari and Gharali [28] have investigated the effect of internal fins on the fluid flow and heat transfer through a rotating straight pipe and a stationary curved pipe. Ishigaki [29–31] examined flow and heat transfer in a rotating curved pipe and investigated the effect of coriolis force in complicating the flow structure. Heat transfer and fluid flow in a curved annular pipe has been studied in the fully developed region by Karahalios [32], Petrakis and Karahalios [33]. Also, the effect of catheterization on the flow characteristics in a curved artery was studied by Karahalios [34], Ebadian [35], Jayaraman and Tiwari [36] and Dash et al. [37].

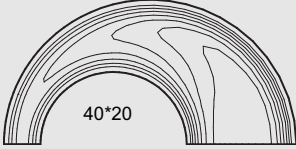
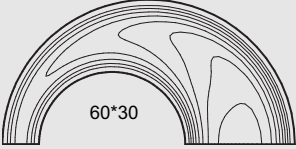
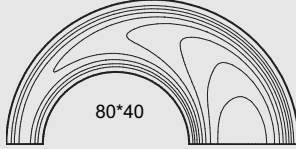
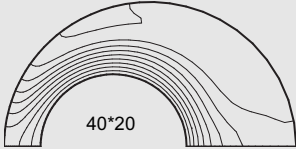
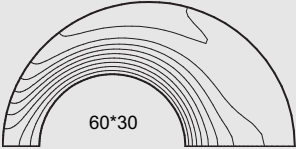
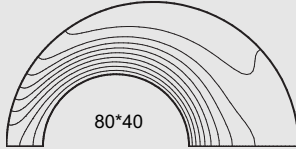
Here, the flow and heat transfer inside an eccentric curved annulus is studied for the first time using a second order finite difference method based on the projection algorithm [38] to solve the governing equations including the continuity, full Navier–Stokes, and energy equations on a bipolar-toroidal coordinate system. The flow is assumed to be hydrodynamically and thermally fully developed and four different thermal boundaries are taken into account consisting of the inner pipe insulated and the outer pipe either at the constant temperature or at the constant heat flux and vice versa. Due to the presence of the symmetrical flow field, it is sufficient to solve only the upper or lower half of the domain. The effects of the governing non-dimensional parameters, such as Dean number, κ_{LC} , Reynolds number, Re , curvature ratio, λ , and eccentricity, E , on the flow characteristics involving axial flow, secondary flow pattern, friction factor, temperature profiles and Nusselt number are investigated in detail. Furthermore, the possibility of the heat transfer rate augmentation in the eccentric curved annuli is discussed.

different researchers. For example McConalogue and Srivastava [20] proposed the parameter $D = (Ga^2/\mu)(2a^3/\nu^2R)^{1/2}$, where G is the constant pressure gradient along the pipe. This parameter relates to K as $D = 4K^{1/2}$. By this definition of Dean number, the upper limit of

2. Governing equations

Here incompressible viscous fluid flow and heat transfer are studied in eccentric curved annuli (Fig. 1) taking into account the

Table 1
Grid independency test in three different mesh sizes of 40×20 , 60×30 , and 80×40 at $Re = 320$ and $Pr = 1$.

Axial velocity contours			
Temperature contours			
Friction factors	0.44040713	0.43747213	0.42709157
Nusselt numbers	5.551282	5.450651	5.283492

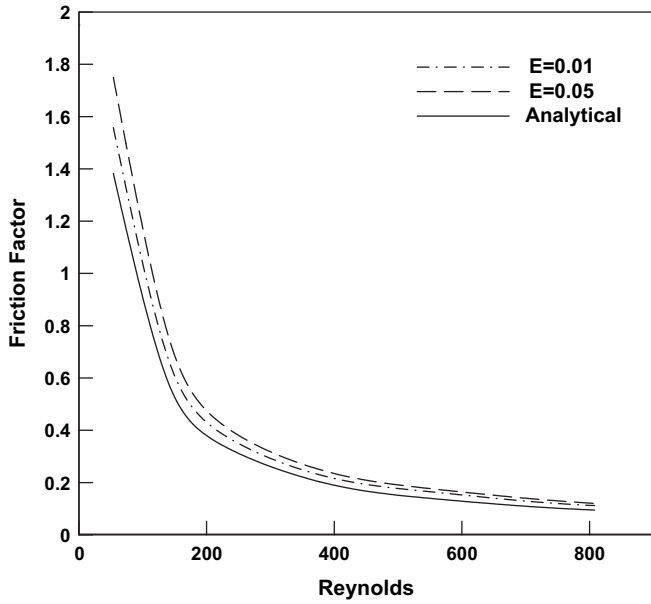


Fig. 3. Comparison of friction factor of concentric straight pipe with slightly eccentric and curved pipe at $E = 0.05$ ($\lambda = 15$) and $E = 0.01$ ($\lambda = 75$) for $N = 0.5$.

hydrodynamically and the thermally fully developed region. To obtain the steady state solution of the problem, the transient form of the governing equations consisting of the continuity, full Navier–Stokes, and the energy equations are derived in a bipolar-toroidal coordinate system which is compatible both with the geometry of the current problem and with the present implemented finite difference scheme. Therefore, the governing equations can be expressed as the continuity

$$\frac{1}{h^3 \sinh \eta} \left[\frac{\partial}{\partial \xi} (h^2 \sinh \eta u) + \frac{\partial}{\partial \eta} (h^2 \sinh \eta v) \right] = 0 \quad (1)$$

the momentum in the ξ direction

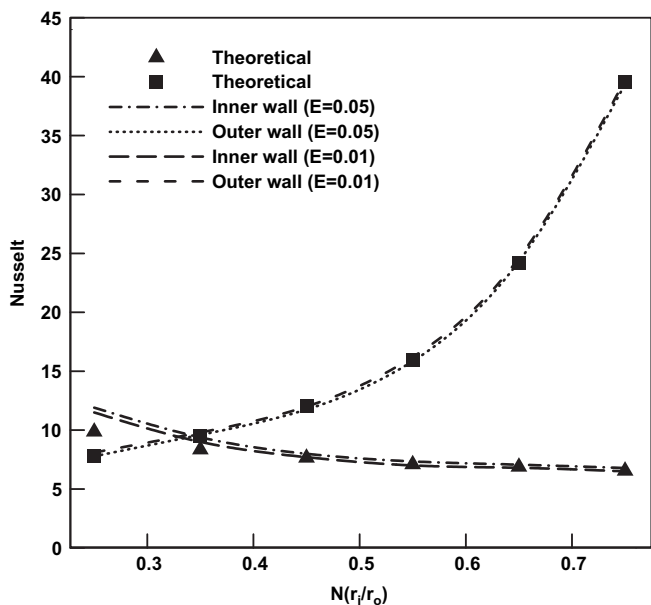


Fig. 4. Comparison of constant heat flux Nusselt number of concentric straight pipe with slightly eccentric and curved pipe at $E = 0.05$ ($\lambda = 15$) and $E = 0.01$ ($\lambda = 75$) for $N = 0.5$.

$$\begin{aligned} \rho \frac{\partial u}{\partial t} + \rho \left(\frac{u \partial u}{h \partial \xi} + \frac{v \partial u}{h \partial \eta} + \frac{uv \partial h}{h^2 \partial \eta} - \frac{v^2 \partial h}{h^2 \partial \xi} - \frac{w^2}{h^2 \sinh \eta} \frac{\partial (h \sinh \eta)}{\partial \xi} \right) + \frac{1 \partial p}{h \partial \xi} \\ = \frac{\mu \partial}{h \partial \xi} \left(\frac{1}{h^3} \frac{\partial}{\partial \xi} (h^2 u) \right) + \frac{\mu \partial}{h \partial \xi} \left(\frac{1}{h^3 \sinh \eta} \frac{\partial}{\partial \eta} (h^2 \sinh \eta v) \right) \\ - \frac{\mu}{h^2 \sinh \eta} \frac{\partial}{\partial \eta} \left(\frac{\sinh \eta}{h} \frac{\partial}{\partial \xi} (h v) \right) + \frac{\mu}{h^2 \sinh \eta} \frac{\partial}{\partial \eta} \left(\frac{\sinh \eta}{h} \frac{\partial}{\partial \eta} (h u) \right) \end{aligned} \quad (2)$$

the momentum in the η direction

$$\begin{aligned} \rho \frac{\partial v}{\partial t} + \rho \left(\frac{u \partial v}{h \partial \xi} + \frac{v \partial v}{h \partial \eta} + \frac{uv \partial h}{h^2 \partial \xi} - \frac{u^2 \partial h}{h^2 \partial \eta} - \frac{w^2}{h^2 \sinh \eta} \frac{\partial (h \sinh \eta)}{\partial \eta} \right) + \frac{1 \partial p}{h \partial \eta} \\ = \frac{\mu \partial}{h \partial \eta} \left(\frac{1}{h^3} \frac{\partial}{\partial \xi} (h^2 u) \right) + \frac{\mu \partial}{h \partial \eta} \left(\frac{1}{h^3 \sinh \eta} \frac{\partial}{\partial \eta} (h^2 \sinh \eta v) \right) \\ + \frac{\mu}{h^2 \sinh \eta} \frac{\partial}{\partial \xi} \left(\frac{\sinh \eta}{h} \frac{\partial}{\partial \xi} (h v) \right) - \frac{\mu}{h^2 \sinh \eta} \frac{\partial}{\partial \xi} \left(\frac{\sinh \eta}{h} \frac{\partial}{\partial \eta} (h u) \right) \end{aligned} \quad (3)$$

the momentum in the φ direction

$$\begin{aligned} \rho \frac{\partial w}{\partial t} + \rho \left(\frac{u \partial w}{h \partial \xi} + \frac{v \partial w}{h \partial \eta} + \frac{uw}{h^2 \sinh \eta} \frac{\partial (h \sinh \eta)}{\partial \xi} \right. \\ \left. + \frac{vw}{h^2 \sinh \eta} \frac{\partial (h \sinh \eta)}{\partial \eta} \right) + \frac{1}{h \sinh \eta} \frac{\partial p}{\partial \varphi} \\ = + \frac{\mu}{h^2} \frac{\partial}{\partial \xi} \left(\frac{1}{h} \frac{\partial}{\partial \xi} (h w) \right) + \frac{\mu}{h^2} \frac{\partial}{\partial \eta} \left(\frac{1}{h \sinh \eta} \frac{\partial}{\partial \eta} (h \sinh \eta w) \right) \end{aligned} \quad (4)$$

the energy equation

$$\begin{aligned} \frac{\partial T}{\partial t} + \frac{u \partial T}{h \partial \xi} + \frac{v \partial T}{h \partial \eta} + \frac{w}{h \sinh \eta} \frac{\partial T}{\partial \varphi} = \frac{k / \rho c_p}{h^3 \sinh \eta} \left[\frac{\partial}{\partial \xi} \left(h \sinh \eta \frac{\partial T}{\partial \xi} \right) \right. \\ \left. + \frac{\partial}{\partial \eta} \left(h \sinh \eta \frac{\partial T}{\partial \eta} \right) \right] \end{aligned} \quad (5)$$

where u is the velocity in the ξ direction, v the velocity in the η direction, w the velocity in the φ direction, ρ the density, μ the viscosity, k the conductivity, c_p the constant pressure specific heat, p the pressure, and T the temperature. In addition, h is the scale factor of the bipolar-toroidal coordinate system and can be defined as

$$\begin{aligned} h = h_\xi = h_\eta = \frac{a}{\cosh \eta - \cos \xi} \\ h_\varphi = h \sinh \eta \end{aligned} \quad (6)$$

where, a is the pole of bipolar coordinate and the radius of curvature, which is expressed as

$$\begin{aligned} a = r_i \sinh \eta_i \\ a = r_o \sinh \eta_o \end{aligned} \quad (7)$$

At a given fully developed region, the outer wall and the inner wall of the curved eccentric annulus can be expressed respectively in a bipolar-toroidal coordinate system as

$$\begin{aligned} \eta_o = \cosh^{-1} \left\{ \frac{N(1 - E^2) + (1 + E^2)}{2E} \right\} \\ = \text{Ln} \left\{ \frac{N(1 - E^2) + (1 + E^2)}{2E} \right. \\ \left. + \sqrt{\left(\frac{N(1 - E^2) + (1 + E^2)}{2E} \right)^2 - 1} \right\} \end{aligned} \quad (8)$$

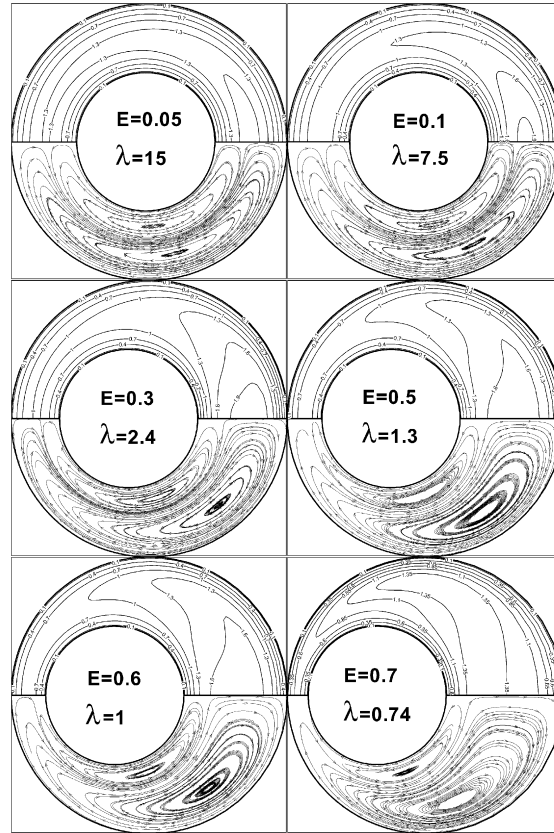


Fig. 5. Axial velocity contour lines (upper half) and secondary flow field (lower half) at six different eccentricities and curvatures of eccentric curved annulus for $Re = 200$ and $N = 0.5$.

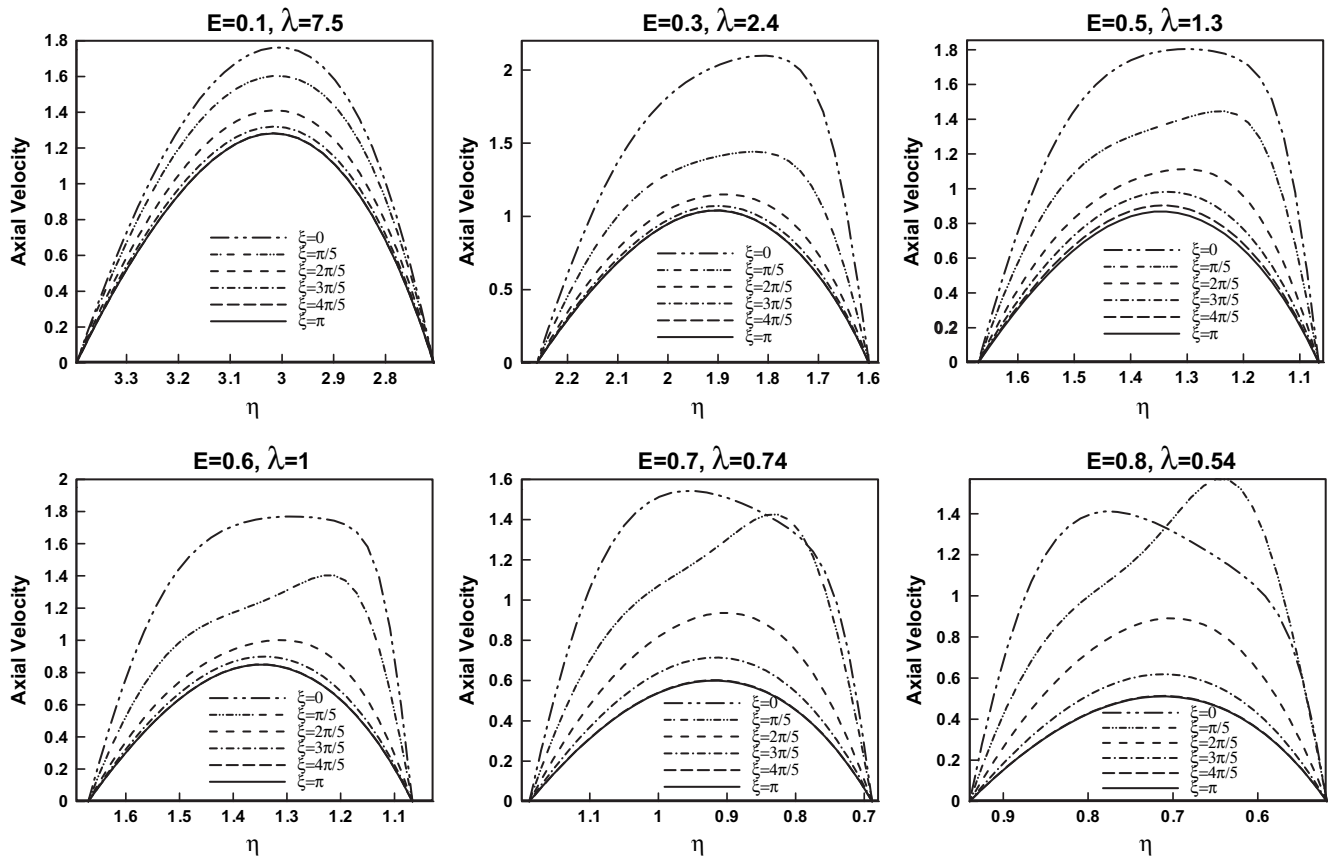


Fig. 6. Axial velocity profiles at six different angles of $0, \pi/5, 2\pi/5, 3\pi/5, 4\pi/5,$ and π for six different eccentricities, $Re = 200$, and $N = 0.5$.

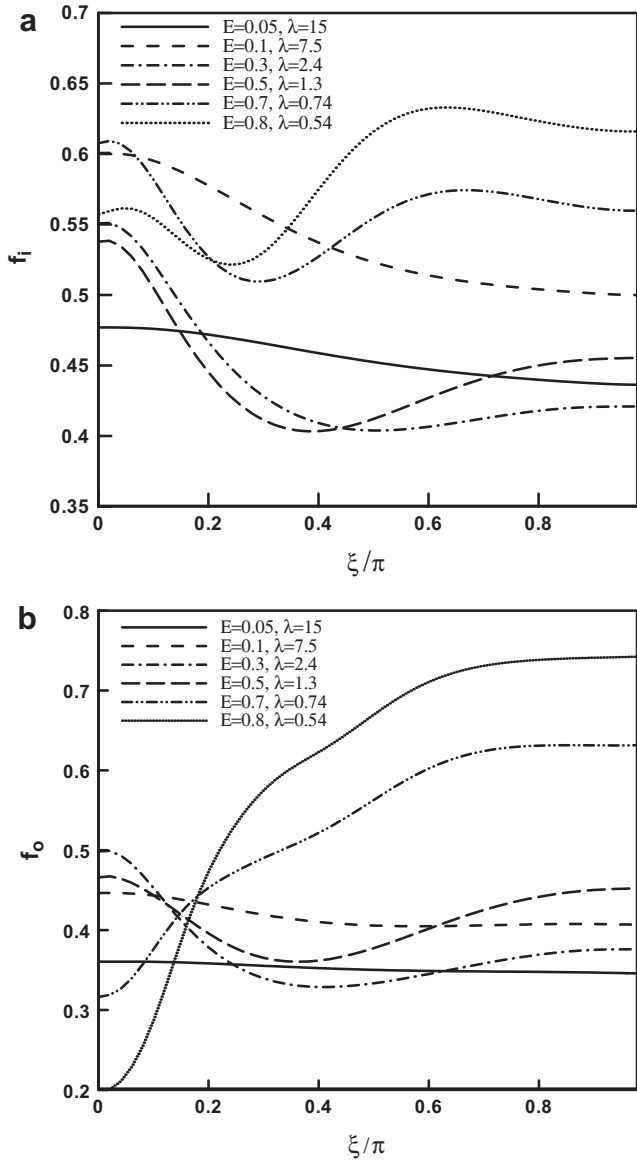


Fig. 7. Circumferential local friction factor on inner (a) and outer (b) pipes of eccentric curved annulus for six different eccentricities, $Re = 200$, and $N = 0.5$.

$$\eta_i = \cosh^{-1} \left\{ \frac{N(1 + E^2) + (1 - E^2)}{2NE} \right\} = \ln \left\{ \frac{N(1 + E^2) + (1 - E^2)}{2NE} + \sqrt{\left(\frac{N(1 + E^2) + (1 - E^2)}{2NE} \right)^2 - 1} \right\} \quad (9)$$

where E is the non-dimensional eccentricity and N is the radius ratio.

$$E = \frac{e}{r_o - r_i}, \quad N = \frac{r_i}{r_o} \quad (10)$$

The local friction factor in the eccentric curved annulus can be expressed based on the outer and inner pipe walls using the following relations

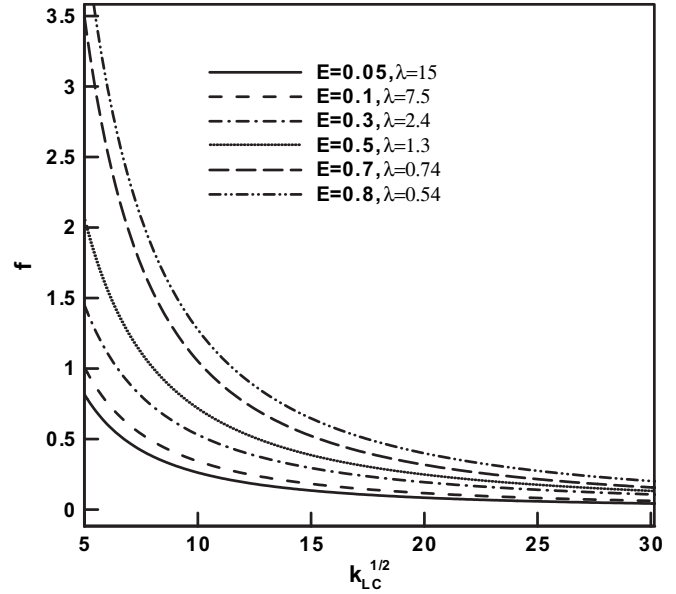


Fig. 8. Average friction factor versus square root of Dean number at six different eccentric curved annuli for $N = 0.5$.

$$f_o = \frac{1}{h_{\eta_o}} \left[\frac{\partial w}{\partial \eta} \right]_{\eta_o} \frac{8}{\rho w^2} \quad \text{at outer pipe} \quad (11)$$

$$f_i = \frac{1}{h_{\eta_i}} \left[\frac{\partial w}{\partial \eta} \right]_{\eta_i} \frac{8}{\rho w^2} \quad \text{at inner pipe}$$

The mean friction factor can be determined in terms of the above mentioned local friction factors as

$$f = \frac{Nf_i + f_o}{1 + N} \quad (12)$$

The boundary condition for the velocity is no-slip condition at the walls and for the thermal boundary either the inner pipe or the outer pipe is adiabatic while the other one is considered to be either at the constant temperature or at the constant heat flux. Therefore, four different thermal boundaries are taken into account in the current study. For the constant temperature at the outer or inner wall, the thermal boundaries are written respectively as

$$T(\eta_o, \xi, \varphi) = T_o \text{ or } \theta_o = 0, \quad \text{where } \theta = \frac{T_o - T}{T_o - T_m} \quad \text{for outer wall}$$

$$T(\eta_i, \xi, \varphi) = T_i \text{ or } \theta_i = 0, \quad \text{where } \theta = \frac{T_i - T}{T_i - T_m} \quad \text{for inner wall} \quad (13)$$

For the constant heat flux thermal boundary at the outer or inner wall, the boundary conditions are expressed respectively as

$$\frac{\partial \theta}{\partial \eta} \Big|_{\eta_i} = 1 \quad \text{for inner wall, where } \theta = \frac{\bar{T}_i - T}{q_w^i D_h / k}$$

$$\frac{\partial \theta}{\partial \eta} \Big|_{\eta_o} = 1 \quad \text{for outer wall, where } \theta = \frac{\bar{T}_o - T}{q_w^o D_h / k} \quad (14)$$

where, \bar{T}_i and \bar{T}_o are the average wall temperatures of inner and outer wall respectively. On the other hand, the fully developed conditions for the axial velocity and the temperature profiles have to be applied. In the hydrodynamically fully developed region, the axial velocity profile remains unchanged in the axial direction and it can be represented as

$$\frac{\partial w}{\partial \varphi} = 0. \quad (15)$$

However, in the thermally fully developed region, depending on the thermal boundary conditions applied on the curved annulus

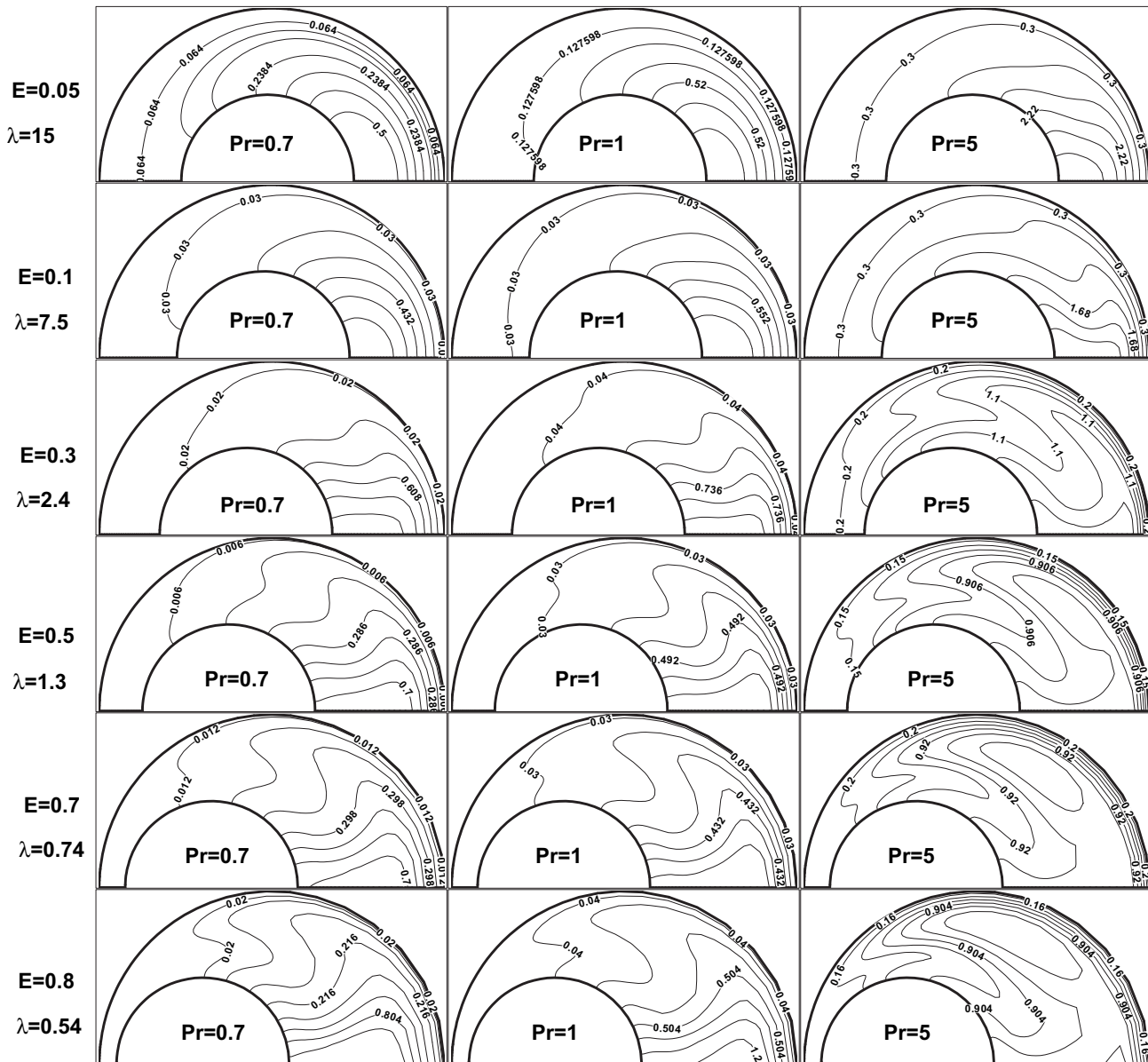


Fig. 9. Temperature contour lines for three Prandtl numbers at six different eccentricities and curvatures of eccentric curved annulus and $N = 0.5$ when inner pipe is insulated and outer pipe is at constant temperature.

walls, the corresponding fully developed conditions must satisfy. The thermally fully developed conditions for the constant temperature at the inner wall or at the outer wall of the annulus can be expressed respectively as

$$\frac{\partial T}{\partial \varphi} = \frac{\partial T_m}{\partial \varphi} = \frac{2\pi r_i q'' h(\xi, \eta_i) \sinh \eta_i}{\rho c_p A w_m} \tag{16}$$

$$\frac{\partial T}{\partial \varphi} = \frac{\partial T_m}{\partial \varphi} = \frac{2\pi r_o q'' h(\xi, \eta_o) \sinh \eta_o}{\rho c_p A w_m}$$

where T_m is the bulk temperature and w_m the mean axial velocity, and A the annular cross sectional area of the curved annulus. They are defined as

$$w_m = \int_0^\pi \int_{\eta_o}^{\eta_i} h^2 w d\eta d\xi / \frac{\pi}{2} (r_o^2 - r_i^2) \tag{17}$$

$$T_m = \int_0^\pi \int_{\eta_o}^{\eta_i} h^2 T w d\eta d\xi / \frac{\pi}{2} (r_o^2 - r_i^2) w_m \tag{18}$$

The fully developed conditions for the constant heat flux at the inner wall or at the outer wall of the curved annulus can be expressed respectively as

$$\frac{\partial T}{\partial \varphi} = \frac{T_i - T}{T_i - T_m} \frac{\partial T_m}{\partial \varphi} \text{ at the inner wall}$$

$$\frac{\partial T}{\partial \varphi} = \frac{T_o - T}{T_o - T_m} \frac{\partial T_m}{\partial \varphi} \text{ at the outer wall} \tag{19}$$

For the four cases considered here including the inner pipe insulated and the outer pipe either at the constant heat flux or at the constant temperature or the outer pipe insulated and the inner pipe either at the constant heat flux or at the constant temperature, the local dimensionless heat transfer rate in an eccentric curved annulus can be determined as

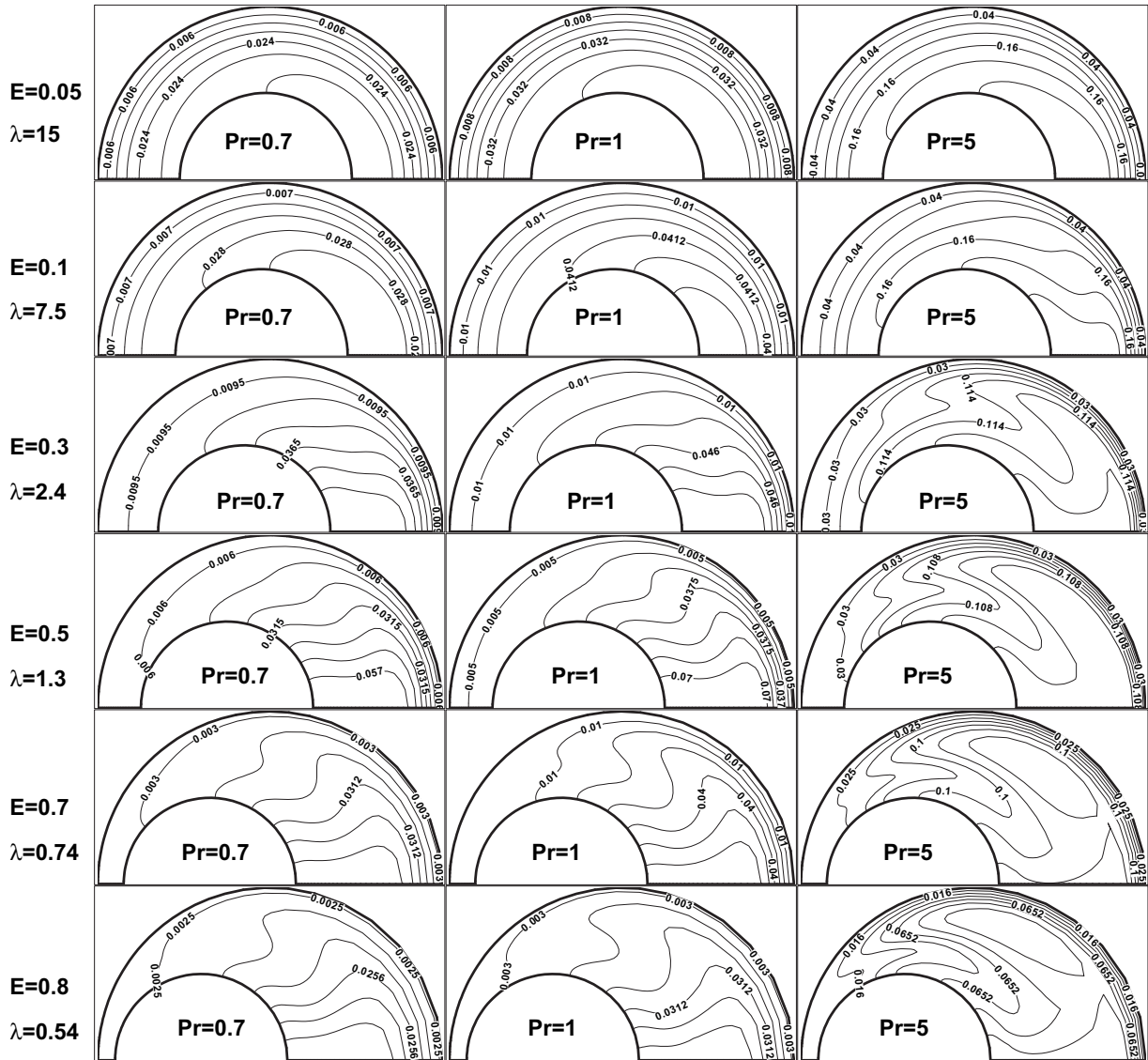


Fig. 10. Temperature contour lines for three Prandtl numbers at six different eccentricities and curvatures of eccentric curved annulus and $N = 0.5$ when inner pipe is insulated and outer pipe is at constant heat flux.

$$Nu_{\xi} = -\frac{D_h}{h_{\eta_i}} \frac{1}{T_i - T_m} \left[\frac{\partial T}{\partial \eta} \right]_{\eta_i} \quad \text{for constant temperature}$$

at inner wall

$$Nu_{\xi} = \frac{D_h}{h_{\eta_o}} \frac{1}{T_o - T_m} \left[\frac{\partial T}{\partial \eta} \right]_{\eta_o} \quad \text{for constant temperature at outer wall} \quad (20)$$

$$Nu_{\xi} = \frac{D_h}{k} \frac{\dot{q}''_i}{\bar{T}_i - T_m} \quad \text{for constant heat flux at inner wall}$$

$$Nu_{\xi} = \frac{D_h}{k} \frac{\dot{q}''_o}{\bar{T}_o - T_m} \quad \text{for constant heat flux at outer wall} \quad (21)$$

for constant heat flux at outer wall

In the four different cases of thermal boundaries, the average Nusselt number can be expressed as

$$Nu = \frac{1}{\pi r_i} \int_0^{\pi} Nu_{\xi} h_{\xi} d\xi \quad \text{for inner wall} \quad (22)$$

$$Nu = \frac{1}{\pi r_o} \int_0^{\pi} Nu_{\xi} h_{\xi} d\xi \quad \text{for outer wall}$$

Furthermore, in any kind of curved pipe flows, there are three common important non-dimensional physical parameters including the Reynolds number, the Dean number, and the non-dimensional curvature from which two of them are independent and are used to analyze different corresponding physical phenomena. They can be defined as

Reynolds number:

$$Re = \frac{\rho W_m d_h}{\mu} \quad (23)$$

Non-dimensional curvature:

$$\lambda = \frac{a}{d_h} = \frac{\sinh \eta_o}{2(1-N)} = \frac{N \sinh \eta_i}{2(1-N)} \quad (24)$$

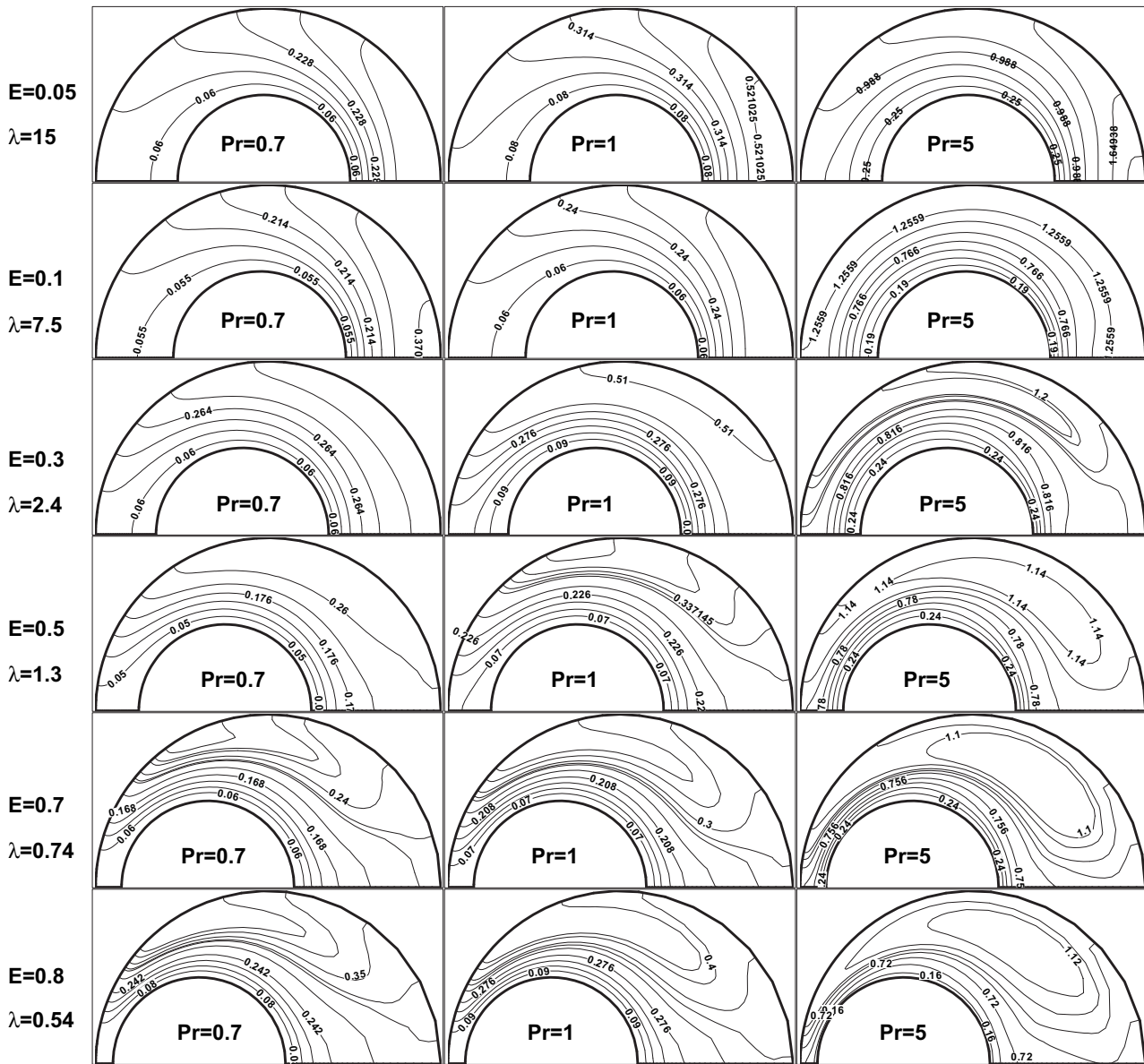


Fig. 11. Temperature contour lines for three Prandtl numbers at six different eccentricities and curvatures of eccentric curved annulus and $N = 0.5$ when outer pipe is insulated and inner pipe is at constant temperature.

Dean number:

$$K_{LC} = \frac{Re}{\lambda^{1/2}} \tag{25}$$

As is evident from Eq. (23), using the toroidal coordinate system based on the bipolar coordinate, the curvature depends on the eccentricity for a specified radius ratio (N). Therefore, the variation of the eccentricity results in the variation of the curvature. Hence, to investigate the effect of eccentricity and curvature on the flow and temperature field in detail, six different cases are considered in the Results and discussion section.

3. Numerical method

The governing equations are solved using forward in time and central in space finite difference method based on the projection algorithm [38]. Since the steady state solution of the problem is

considered, the unsteady terms in the equations must vanish. Therefore, the following convergence conditions must be applied

$$\left\{ \max \left| \frac{\partial u}{\partial t} \right|, \max \left| \frac{\partial v}{\partial t} \right|, \max \left| \frac{\partial w}{\partial t} \right| \right\} \leq \varepsilon \tag{26}$$

where ε is a small value close to zero depending on the accuracy of the solution. Here it is taken into account as 10^{-6} . In the projection algorithm the momentum equations are split into two fractions using an auxiliary velocity, v^* , as follows

$$\frac{\vec{V}^* - \vec{V}^n}{\Delta t} + ((\vec{V} \cdot \nabla) \cdot \vec{V})^n = \nu (\nabla^2 \vec{V})^n \tag{27}$$

$$\frac{\vec{V}^{n+1} - \vec{V}^*}{\Delta t} + \frac{\nabla p^{n+1}}{\rho} = 0 \tag{28}$$

$$\nabla \cdot \vec{V}^{n+1} = 0 \tag{29}$$

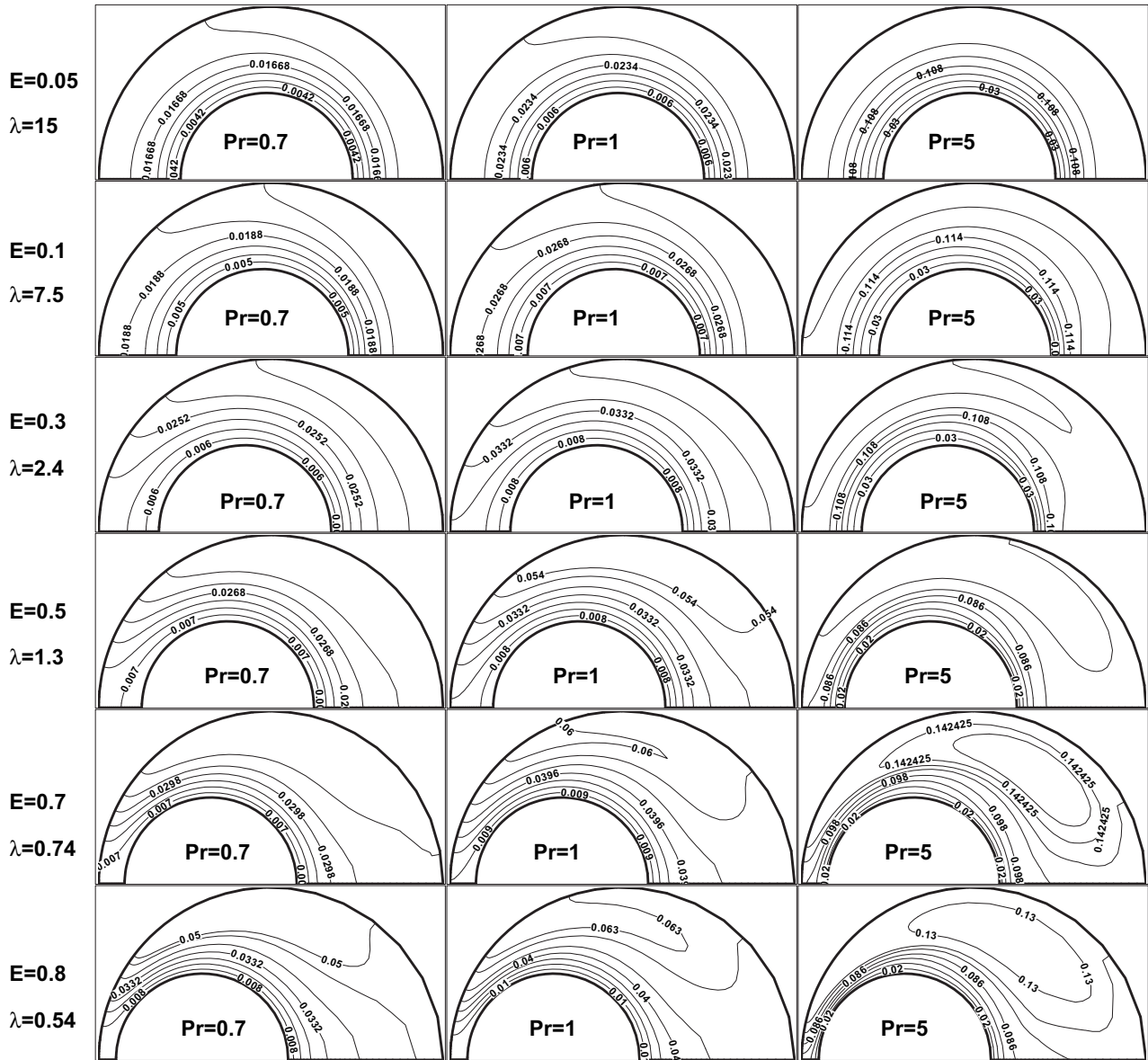


Fig. 12. Temperature contour lines for three Prandtl numbers at six different eccentricities and curvatures of eccentric curved annulus and $N = 0.5$ when outer pipe is insulated and inner pipe is at constant heat flux.

$$\nabla^2 p^{n+1} = \frac{\rho}{\Delta t} \nabla \cdot \vec{V}^* \quad (30)$$

Furthermore, it can be easily proven that the pressure field in the projection algorithm is independent of the boundary values of v^* . Therefore, by taking a suitable boundary value of v^* equal to the physical velocity values at the boundaries, the following Neumann condition for the pressure at all boundaries can be applied.

$$\frac{\partial p}{\partial n} = 0 \quad (31)$$

Due to the explicit discretization, the following stability conditions have to be applied

$$\frac{4\Delta t}{\min\{(h_\varphi d\varphi)^2, (h_\xi d\xi)^2, (h_\eta d\eta)^2\}} \leq 1, \quad \frac{1}{2} \max(u^2 + v^2) \text{Re} \Delta t \leq 1 \quad (32)$$

where, Re is the Reynolds number, $\text{Re} = \rho w_m D_h / \mu$, and Δt is the marching time step.

The staggered grid is used to discretize the upper half domain of the curved annulus in the η and in the ξ directions. For the domain defined in the bipolar-toroidal coordinate system (Fig. 2a), the η varies between η_i and η_o and the ξ varies between 0 and π . Therefore, the computational domain shown in Fig. 2b is divided into uniform space steps in the η and the ξ directions.

4. Grid independency test and code accuracy

The second order numerical code developed here is run on the three different meshes of 40×20 , 60×30 , and 80×40 to study its accuracy and conservative property. The numerical results obtained are shown in Table 1 where the contours of the axial velocity and the temperature field along with the friction factors and the heat transfer rates are compared in the forgoing three meshes. As is evident from the table, the numerical results obtained in the three

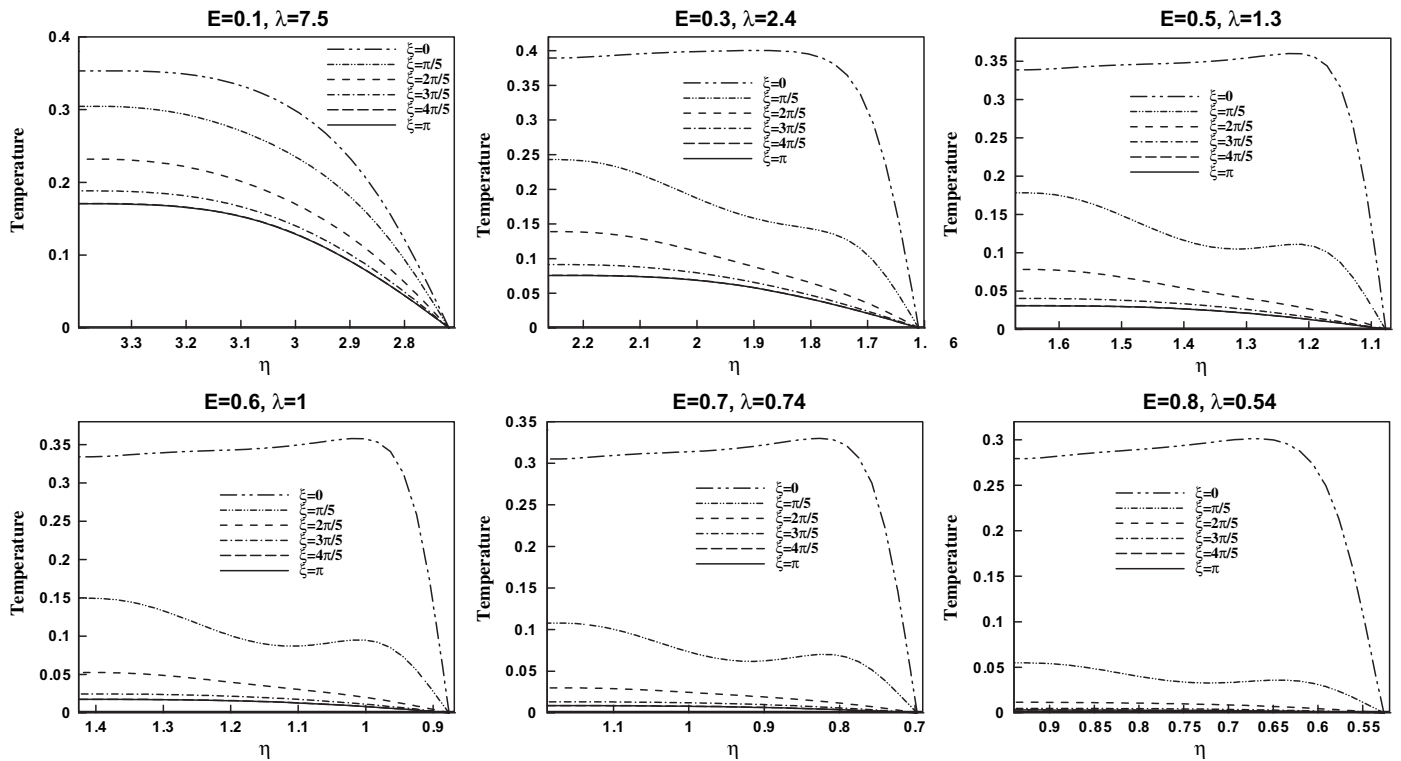


Fig. 13. Temperature profiles at six different angles of $0, \pi/5, 2\pi/5, 3\pi/5, 4\pi/5,$ and π for six different eccentricities ($N = 0.5$) when the inner pipe is insulated and $Pr = 1$.

different mesh sizes indicate a maximum five percent deviation, clearly indicating the well performance of the grid independency of the code.

On the other hand, to check the accuracy of the numerical code, the numerical results obtained for the eccentric curved annulus at

$E = 0.05$ ($\lambda = 15$) and $E = 0.01$ ($\lambda = 75$) are compared with the analytical solutions of the corresponding concentric straight pipe in Figs. 3 and 4 considering the Friction factor and the Nusselt number respectively. As is evident from the figures, the numerical results obtained indicate a very good accuracy of the code. The slight

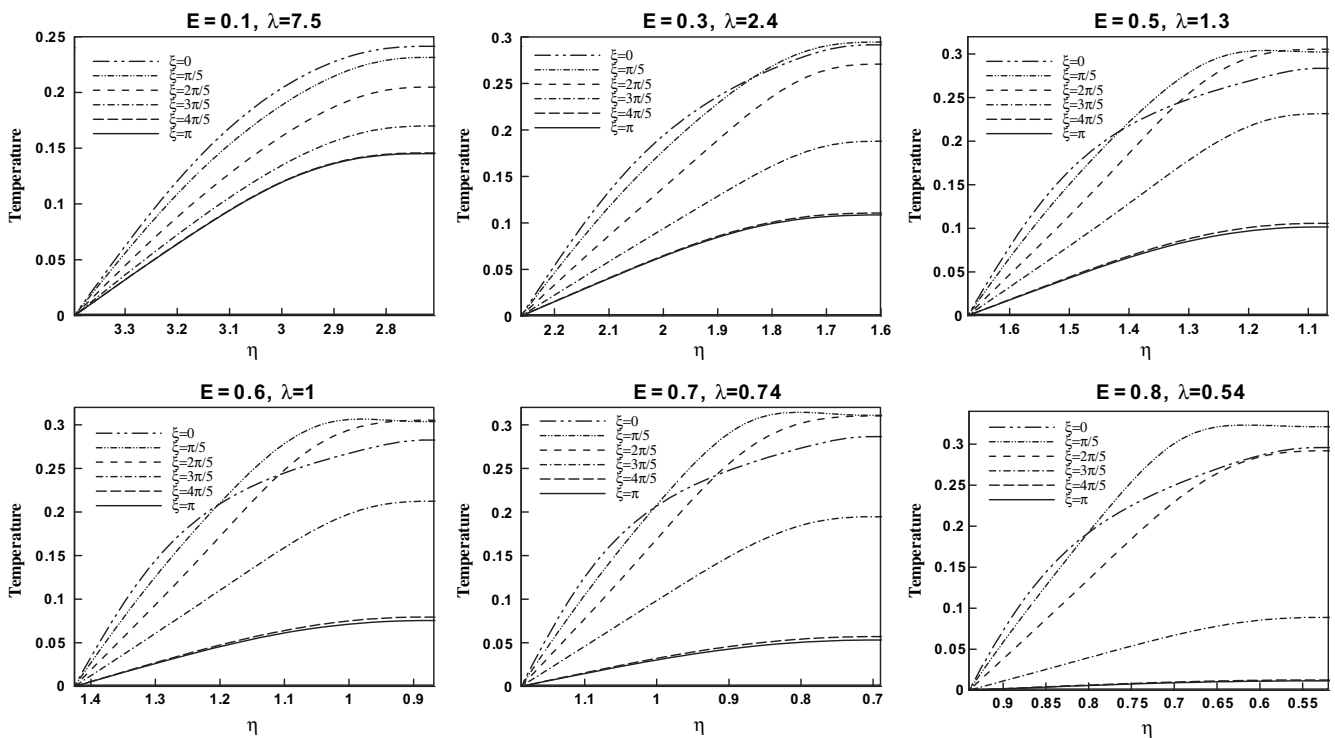


Fig. 14. Temperature profiles at six different angles of $0, \pi/5, 2\pi/5, 3\pi/5, 4\pi/5,$ and π for six different eccentricities ($N = 0.5$) when the outer pipe is insulated and $Pr = 1$.

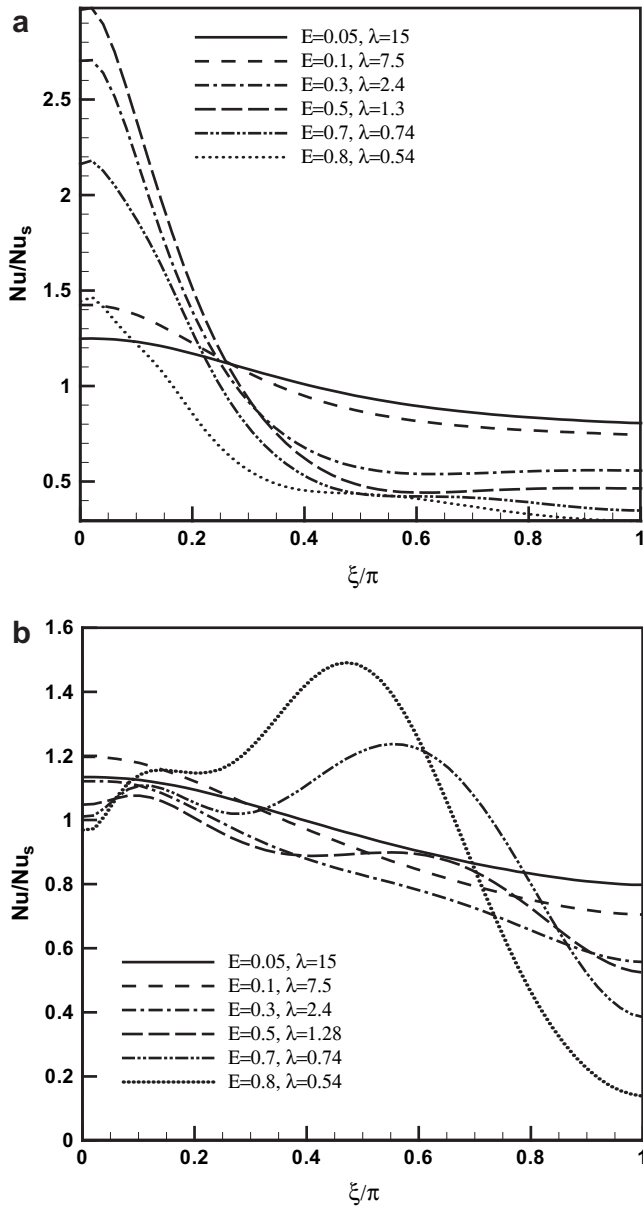


Fig. 15. Inner insulated (a), and outer insulated (b).

difference is due to the presence of the small eccentricity as well as curvature effects in the numerical results. In Fig. 3 as the Reynolds number increases, the Dean number increases and the curvature effect become smaller in the flow field, therefore, the results of the eccentric curved annulus get closer to ones of the straight concentric pipe.

5. Results and discussion

Considering hydrodynamically and thermally fully developed condition in an eccentric curved annulus, it is only required to solve the governing equations in the semi-upper or lower part of the curved annulus cross-section. The physical domain is shown in Fig. 1 which is suitably fit to the bipolar-toroidal coordinate system indicated in Fig. 2a. Also, the finite difference scheme used here can be easily applied due to the availability of uniform orthogonal divisions in the η and the ξ directions as shown in Fig. 2b. It has to

be mentioned that all the numerical results obtained here are carried out using the mesh size 60×30 and the radius ratio of 0.5.

Similar to the fluid flow in curved pipes, the flow inside an eccentric curved annulus develops under the effects of centrifugal, pressure, and inertial forces. The centrifugal forces and the radial pressure gradient due to the curvature cause the secondary flow formation in the curved pipes. Near the walls the values of the velocity are smaller due to the no-slip condition and consequently the centrifugal forces which are directly proportional to the square of the axial velocities become smaller close to the inner and outer curved pipe walls. On the other hand, as the radius of the curvature increases, the centrifugal forces decrease while the pressure forces increase. Hence, the boundary layers near the walls develop from the outer bend toward the inner bend balancing the pressure forces with centrifugal ones. On the contrary, in the core region away from the pipe walls the centrifugal forces are dominant due to the larger velocities and the flow develops from the inner bend where the centrifugal forces larger toward the outer bend. The interaction of the core flow with the two boundary layers generates two pairs of vortices close to the pipe walls. The pair vortex near the inner curved pipe is smaller than the other one near the outer curved pipe due to the stronger boundary layer development on the outer curved pipe wall. This physical phenomenon is clearly shown in Fig. 5 where the semi-lower annulus indicates the secondary flow field and the semi-upper one represents the contours of the axial velocity at six different eccentricities and curvatures. As the eccentricity increases the intensity of the boundary layer flow over the inner curved pipe wall weakens while that over the outer curved pipe wall strengthens. Therefore, the vortex pair due to the inner curved pipe wall becomes smaller and its core shifts towards the wide region of the annulus by increasing the eccentricity. Furthermore, the centrifugal forces push the maximum velocity toward the outer bend comparing with the similar straight annulus as shown in Fig. 5 (the semi-upper annulus). By increasing the eccentricity and decreasing the curvature radius up to $\lambda = 1$, the cores of the two pair vortices generated by the interaction of the core flow from the inner to the outer curvature and the two boundary layers flows from the outer to the inner curvature shift more toward the outer curved region due to the strengthening of the centrifugal forces. This is accompanied with the shifting of the maximum axial velocity location more closely to the outer curved pipe wall compared with the corresponding eccentric straight annulus. However, for $\lambda < 1$ the center of vortices start slightly moving toward the inner curved region and the maximum axial velocity between $\xi = 0$ and $\xi = \pi/6$ shifts toward the inner curved pipe wall instead of outer curved pipe wall. This phenomenon stems from the larger eccentricity effect ($E = 0.7$ and $E = 0.8$) at which the axial velocity values become smaller in the wider region between $\xi = 0$ and $\xi = \pi/6$ and correspondingly the centrifugal forces become weaker than the pressure gradient forces in the curvature direction pushing the maximum axial velocity toward inner curved pipe wall. This physical effect is clearly represented in Fig. 6 where the axial velocity profiles at six different eccentricities and curvatures are shown in the six ξ -directions of $\xi = 0$, $\xi = \pi/5$, $\xi = 2\pi/5$, $\xi = 3\pi/5$, $\xi = 4\pi/5$, and $\xi = \pi$. For the last two cases in Fig. 6, i.e. $E = 0.7$ and $E = 0.8$, the peak of axial velocity profiles at $\xi = 0$ moves toward the inner curved pipe wall in contrast with the other cases. Also in each case the velocity values in the wider region are larger than the narrower one due to the less resistance in the wider region. The local circumferential friction factors on the inner (a) and outer (b) pipe walls are shown in Fig. 7 at six different eccentricities and curvatures. As the numerical results indicate beyond $\lambda = 1$ the maximum local friction factor moves from the outer curved region (between $\xi = 0$ and $\xi = \pi/2$) toward the inner curved region (between $\xi = \pi/2$ and $\xi = \pi$) both on the inner and

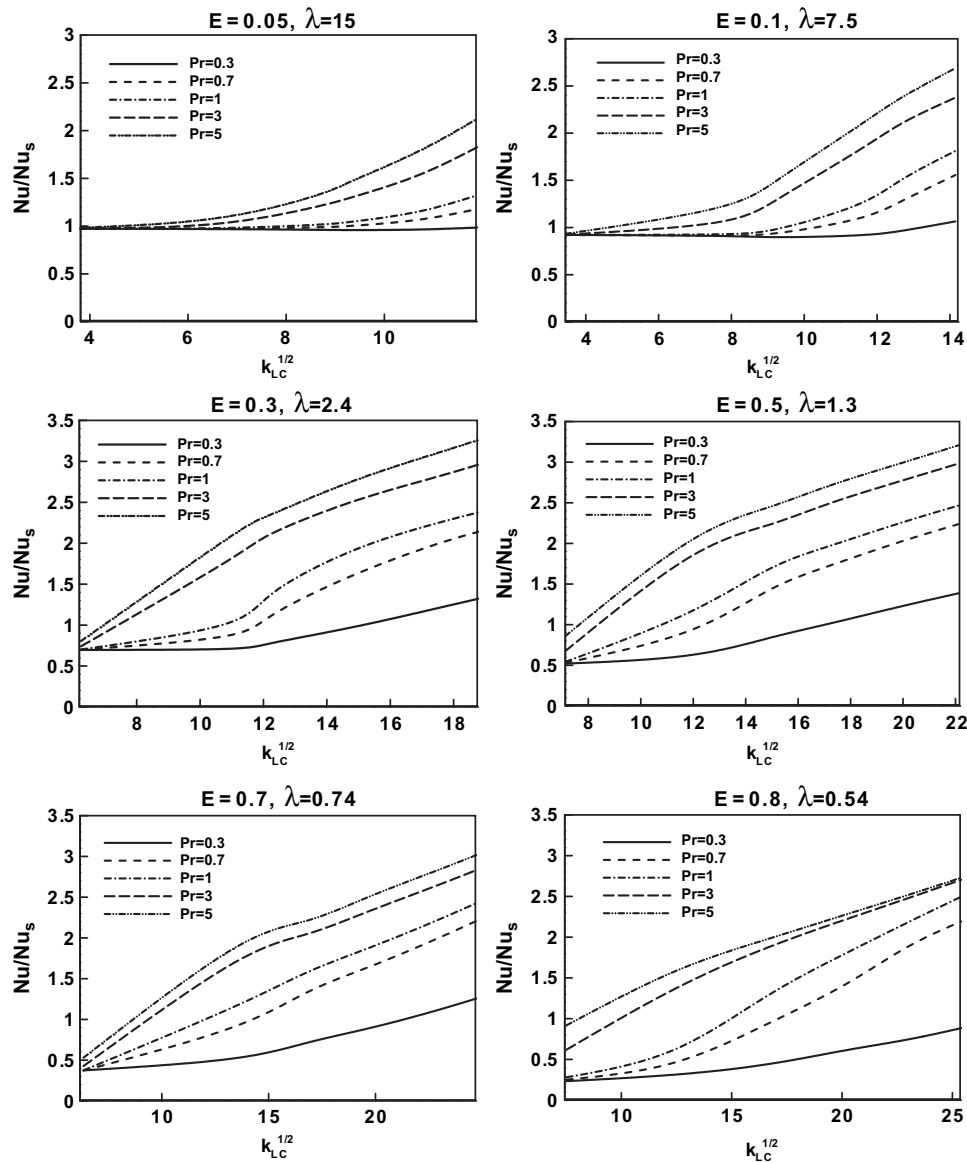


Fig. 16. Nusselt number ratio of straight concentric pipe to eccentric curved annulus for ($N=0.5$) five Prandtl numbers at six different eccentricities and curvatures of eccentric curved annulus when inner pipe is insulated and outer pipe is at constant temperature.

outer pipe walls. In Fig. 8 the average friction factor versus square root of the Dean number are shown for six different eccentricities and curvatures of the eccentric curved annulus. As the eccentricity increases and the curvature radius decreases, the friction factor increases due to the intensifying centrifugal forces. But at a constant eccentricity and curvature radius, the friction factor is inversely proportional to the square root of Dean number.

To study the heat transfer in an eccentric curved annulus, four different cases depending on the different thermal boundary conditions are taken into account. These cases include the constant temperature and the constant heat flux at either outer or inner curved pipe while the inner or the outer pipe is kept thermally insulated. Here, forced convection is taken into account and the effect of gravity is neglected. However, the numerical results shown can be used in the presence of gravity for the pipes with diameters less than or equal four inches where the Richardson number (Gr/Re^2) stay in the dominant range of forced convection considering gases and liquids such as glycerin. In the study by Manglik and Fang [6], it is shown that in the eccentric straight annuli comparing with the

concentric annuli the heat transfer rate decreases as the eccentricity increases. In the present study, it will be indicated that in contrast to the eccentric straight annuli, the heat transfer rate augmentation is possible in the eccentric curved annuli due to the presence of secondary flows generated by the curvature. Figs. 9–12 indicate the temperature contour lines at the three Prandtl numbers of 0.7, 1, and 5 considering each of the four thermal boundary conditions. As the numerical results indicate for the Prandtl numbers larger than one the secondary flow affects strongly on the temperature field due to the larger momentum diffusion and remarkably augments the heat transfer rates comparing with the cases for which the Prandtl number is less than one. Therefore, unlike the eccentric straight annuli, Prandtl number has significant effect on the heat transfer in the eccentric curved annuli. Figs. 13 and 14 show the temperature profiles at six different eccentricities and curvatures taking into account the inner pipe and the outer pipe insulated respectively. Each case involves six profiles at six different ξ -directions. It is clear from Fig. 13 where the inner pipe is insulated that the local heat transfer rate decreases by

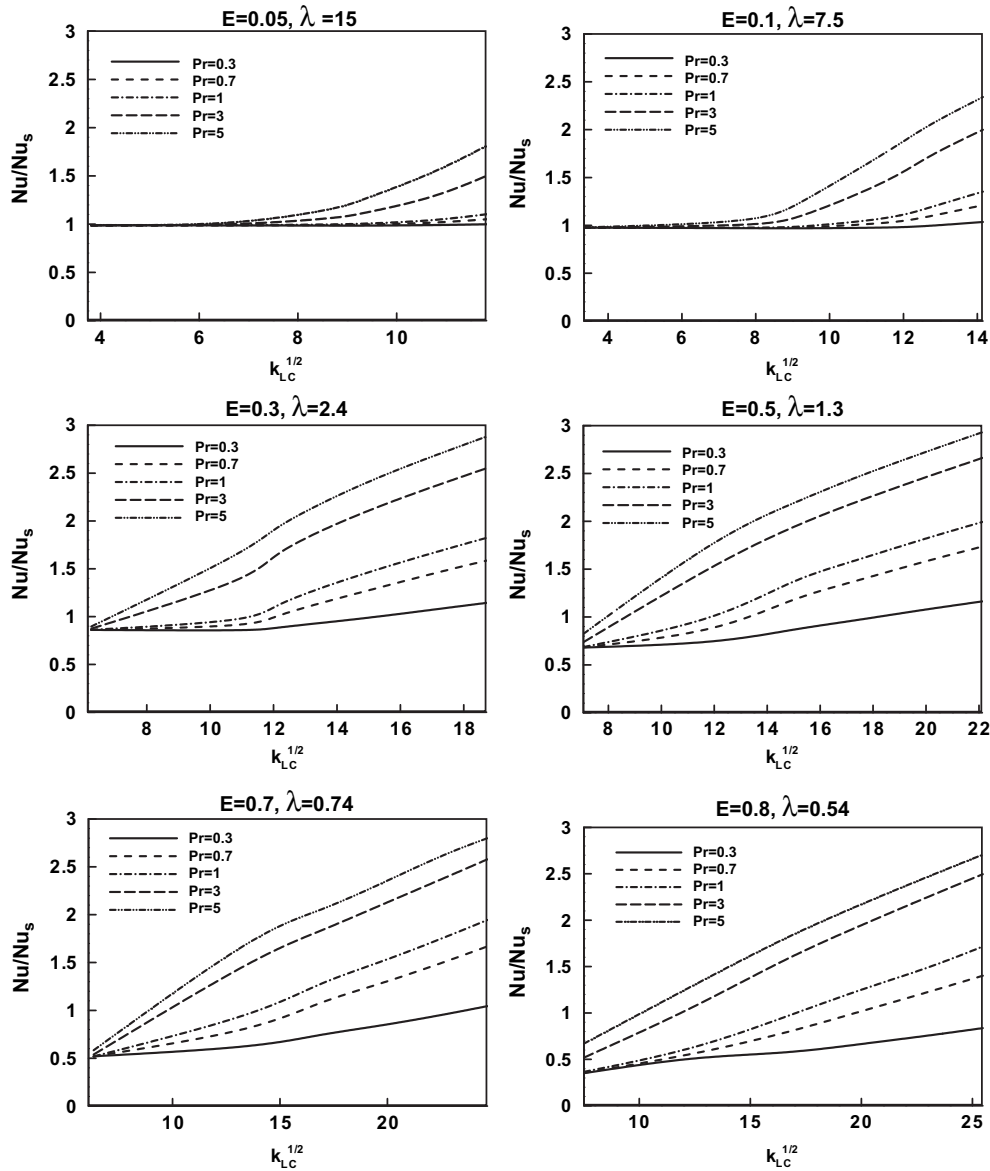


Fig. 17. Nusselt number ratio of straight concentric pipe to eccentric curved annulus for ($N = 0.5$) five Prandtl numbers at six different eccentricities and curvatures of eccentric curved annulus when inner pipe is insulated and outer pipe is at constant heat flux.

moving from the wider region to the narrower region resulting from the thickening of the thermal boundary layers. But in the case of outer insulated pipe (Fig. 14) two different physical trends are observed depending on whether $\lambda \leq 1$ or $\lambda > 1$. In this case as discussed previously, for $\lambda > 1$ at the larger eccentricities ($E = 0.7$ and $E = 0.8$) the centrifugal forces become weaker owing to the reduction of the axial velocity in the wider region while the pressure gradient forces in the curvature direction get stronger resulting from the larger curvature radius. This physical phenomenon causes the peak of velocity field moves from the outer curved pipe wall toward the inner one in some part of the wider region and similarly affects on the temperature field by increasing the local heat transfer rate in the initial stage of the wider region. The local heat transfer rates versus ξ are shown for the inner and outer insulated pipe cases in Fig. 15a and b respectively. As discussed before in Fig. 15a, it is evident that the local heat transfer rate decreases as moving from wider region toward the narrower one, but, this is different in the case of outer insulated pipe (Fig. 15b)

where for $\lambda \leq 1$ the trend of the local heat transfer rate is similar to the previous case and for $\lambda > 1$ first the local heat transfer rate increases as moving from the wider region toward specific point of narrower region then it starts decreasing as shown for the cases of $E = 0.7$ and 0.8 in Fig. 15b.

In Figs. 16–19 the ratio of the average Nusselt number of the eccentric curved annulus to the concentric straight pipe [39] versus the square root of the Dean number is represented for the four thermal boundary cases each at six different eccentricities and curvatures considering five different Prandtl numbers of 0.3, 0.7, 1, 3, and 5. The comparison of the Nusselt numbers in four thermal boundary cases indicates that the Nusselt numbers for the cases with the insulated inner pipe are larger than the ones with the insulated outer pipe due to thinner thermal boundary near the outer curved pipe wall. Furthermore, in each pair cases with the same insulated pipe, the Nusselt numbers for the constant heat flux boundary are less than the corresponding case with the constant temperature boundary. The physical interpretation of this

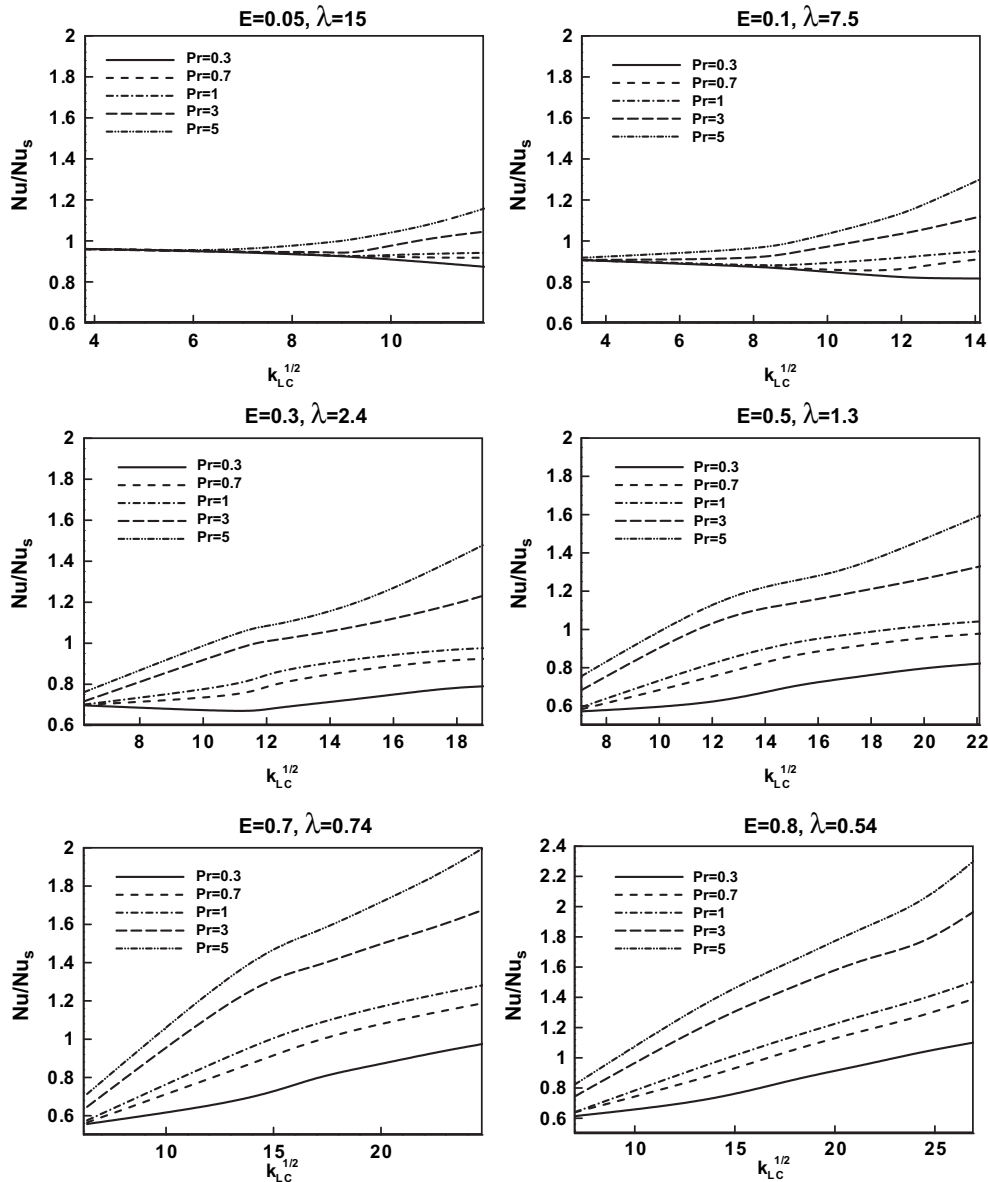


Fig. 18. Nusselt number ratio of straight concentric pipe to eccentric curved annulus ($N=0.5$) for five Prandtl numbers at six different eccentricities and curvatures of eccentric curved annulus when outer pipe is insulated and inner pipe is at constant temperature.

effect stems from the fact that in the cases with the constant temperature boundary conditions, the secondary flow effect on the temperature field is stronger than the cases with heat flux boundary conditions. Also the numerical results indicate that the Nusselt number increases as the eccentricity increases while reducing the curvature radius up to $\lambda = 1$ and $E = 0.6$, beyond that the Nusselt number starts decreasing by increasing the eccentricity and decreasing the radius of curvature. This physical trend results from the reduction of centrifugal forces due to the presence of the larger eccentricities which reduces the axial velocity amount playing major role in the secondary flow field. On the other hand the pressure gradient in the curvature direction becomes stronger and dominant due to the smaller curvature radius ($\lambda < 1$) and pushes the peak of the axial velocity and the temperature field towards the inner pipe wall affecting on the heat transfer rate. Taking into account all the four thermal cases with $Pr > 1$, the Nusselt number of the eccentric curved annulus for the Dean numbers larger than almost 150 increases comparing with the

Nusselt number of the straight concentric pipe. But, for the cases with $Pr < 1$, the heat transfer rate augmentation of the eccentric curved annulus relative to the straight concentric pipe occurs at relatively larger Dean numbers at which the radius of curvature becomes smaller. This is due to lower effect of secondary flow on the temperature field at $Pr < 1$ and larger effect of secondary flow on the temperature field at $Pr \geq 1$.

6. Summary and conclusion

Flow and heat transfer in an eccentric curved annulus are studied numerically by a second order finite difference method based on the projection algorithm. The governing equations including the continuity, full Navier–Stokes, and energy equations are written in the bipolar-toroidal coordinate system which enables the equations to be discretized on an orthogonal uniform staggered mesh used here. Different eccentricities and curvature radii with four different thermal boundaries are considered to study the physics of the

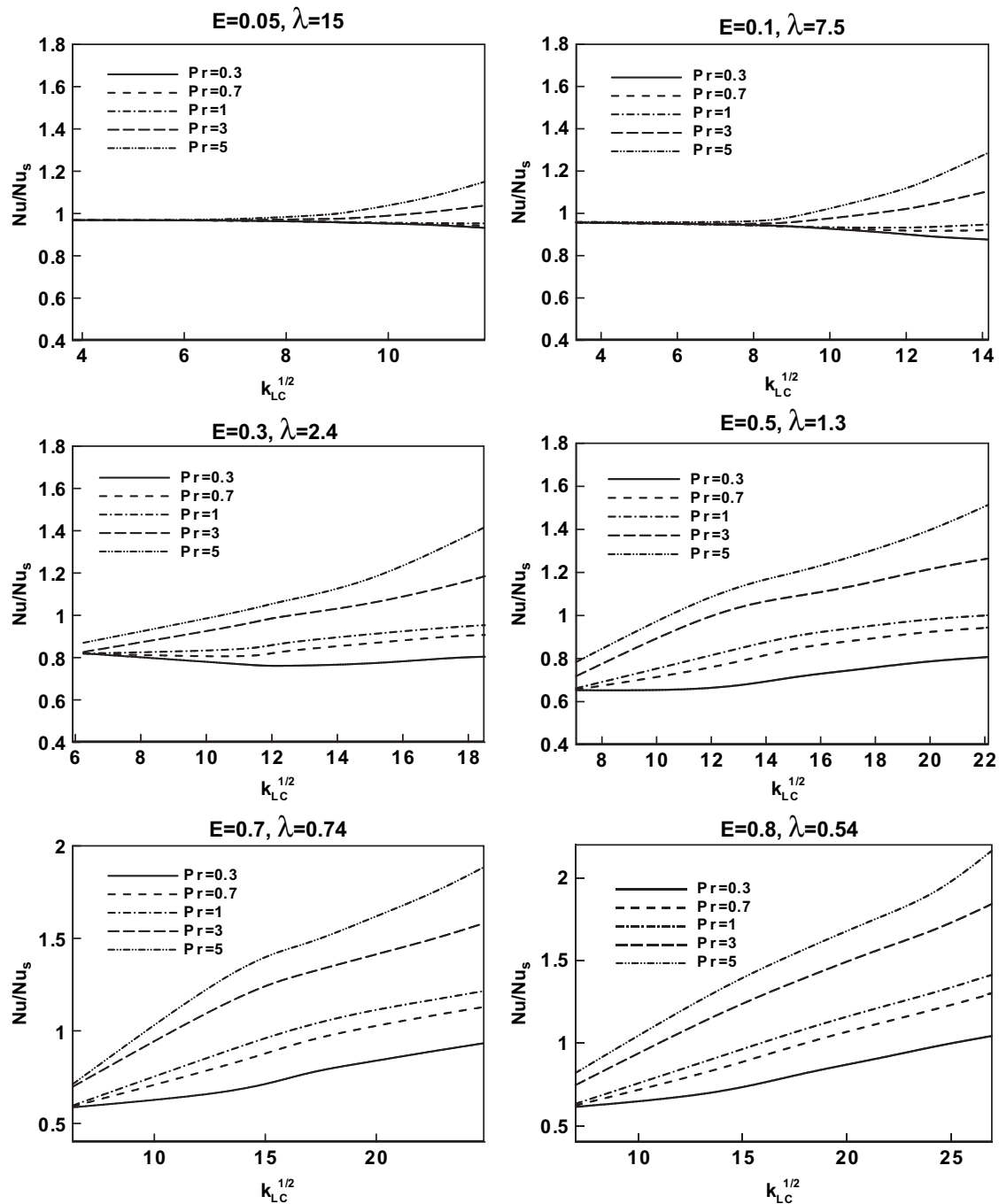


Fig. 19. Nusselt number ratio of straight concentric pipe to eccentric curved annulus ($N=0.5$) for five Prandtl numbers at six different eccentricities and curvatures of eccentric curved annulus when outer pipe is insulated and inner pipe is at constant heat flux.

problem in detail by visualizing different patterns of the flow and temperature fields. The effects of non-dimensional parameters consisting of eccentricity, curvature ratio, Dean number, Prandtl number on the Nusselt number (heat transfer rate) and the friction factor are investigated. It is shown that despite the straight eccentric annuli comparing with eccentric annuli, the heat transfer rate can be augmented in the eccentric curved annuli at the large Dean numbers depending on the eccentricity and the curvature ratio.

References

- [1] L.S. Yao, S.A. Berger, Entry flow in a curved pipe, *J. Fluid Mech.* 67 (1975) 177–196.
- [2] W.T. Snyder, An analysis of slug flow heat transfer in an eccentric annulus, *AIChE J.* 9 (4) (1963) 503–506.
- [3] K.C. Cheng, G.J. Hwang, Laminar forced convection in eccentric annuli, *AIChE J.* 14 (1968) 510–512.
- [4] L. Trombetta, Laminar forced convection in eccentric annuli, *Int. J. Heat Mass Transf.* 14 (1971) 1161–1173.
- [5] K. Susuki, J.S. Szmyd, H. Ohtsuka, Laminar forced convection heat transfer in eccentric annuli, *Heat Transf. Jpn. Res.* 20 (1991) 169–183.
- [6] R.M. Manglik, P.P. Fang, Effect of eccentricity and thermal boundary conditions on laminar fully developed flow in annular ducts, *Int. J. Heat Fluid Flow* 16 (1995) 298–306.
- [7] E.E. Feldman, R.W. Hombeck, J.F. Osterle, A numerical solution laminar developing flow in eccentric annular ducts, *Int. J. Heat Mass Transf.* 25 (2) (1982) 231–241.
- [8] E.E. Feldman, R.W. Hombeck, J.F. Osterle, A numerical solution developing temperature for laminar developing flow in eccentric annular ducts, *Int. J. Heat Mass Transf.* 25 (2) (1982) 243–253.

- [9] C.J. Ho, Y.H. Lin, T.C. Chen, A numerical study of natural convection in concentric and eccentric horizontal cylindrical annuli with mixed boundary conditions, *Int. J. Heat Fluid Flow* 10 (1) (1989) 40–47.
- [10] K. Hirose, T. Hachinohe, Y. Ishii, Natural convection heat transfer in eccentric horizontal annuli between a heated outer tube and a cooled inner tube with different orientation: the case of an elliptical outer tube, *Heat Transf. Asian Res.* 30 (8) (2001) 624–635.
- [11] D. Naylor, H.M. Badr, J.D. Tarasuk, Experimental and numerical study of natural convection between two eccentric tubes, *Int. J. Heat Mass Transf.* 32 (1) (1989) 171–181.
- [12] P. Sathyamurthy, K.C. Karki, S.V. Patankar, Laminar fully developed mixed convection in a vertical eccentric annulus, *Numer. Heat Transf. A* 22 (1) (1992) 71–85.
- [13] D. Choudhury, K. Karki, Laminar mixed convection in a horizontal eccentric annulus, *Numer. Heat Transf. A* 22 (1) (1992) 87–108.
- [14] M.A.I. El-Shaarawi, H.I. Abulhamayel, E.M.A. Mokheimer, Developing laminar forced convection in eccentric annuli, *Heat Mass Transf.* (1998) 353–362.
- [15] I.M.A. El-Shaarawi, A.A.A. Negm, Conjugate natural convection heat transfer in an open-ended vertical concentric annulus, *Numer. Heat Transf. A* 36 (1999) 639–655.
- [16] I.M.A. El-Shaarawi, E.M.A. Mokheimer, H.I. Abulhamayel, Limiting values for free-convection induced flow rates in vertical eccentric annuli with an isothermal boundary, *Numer. Heat Transf. A* 39 (2001) 611–630.
- [17] E.M.A. Mokheimer, M.A.I. El-Shaarawi, Developing mixed convection in vertical eccentric annuli, *Heat Mass Transf.* 41 (2004) 176–187.
- [18] W.R. Dean, Note on the motion of fluid in a curved pipe, *Phil. Mag.* 4 (1927) 208–223.
- [19] W.R. Dean, The stream-line motion of fluid in a curved pipe, *Phil. Mag.* 5 (1928) 673–695.
- [20] D.J. McConalogue, R.S. Srivastava, Motion of fluid in a curved tube, *Proc. R. Soc. Lond. A* 307 (1968) 37–53.
- [21] W.M. Collins, S.C.R. Dennis, The steady motion of a viscous fluid in a curved tube, *Q. J. Mech. Appl. Math.* 28 (2) (1975) 133–156.
- [22] S.C.R. Dennis, Calculation of the steady flow through a curved tube using a new finite-difference method, *J. Fluid Mech.* 99 (1980) 449–467.
- [23] W.Y. SOH, S.A. Berger, Laminar entrance flow in a curved pipe, *J. Fluid Mech.* 148 (1984) 109–135.
- [24] T.J. Pedley, *The Fluid Mechanics of Large Blood Vessels*, Cambridge University Press, 1980.
- [25] S.C.R. Dennis, M. Ng, Dual solutions for steady laminar flow through a curved tube, *Q. J. Mech. Appl. Math.* 35 (1982) 305–324.
- [26] H. Ito, Flow in curved pipes, *JSME Int. J.* 30 (1987) 543–552.
- [27] H.C. Kao, Some aspects of bifurcation structure of laminar flow in curved ducts, *J. Fluid Mech.* 243 (1992) 519–539.
- [28] M.R.H. Nobari, K. Gharali, A numerical study of flow and heat transfer in internally finned rotating straight pipes and stationary curved pipes, *Int. J. Heat Mass Transf.* 49 (2006) 1185–1194.
- [29] H. Ishigaki, Fundamental characteristics of laminar flows in a rotating curved pipe, *Trans. JSME* 59-561-B (1993) 1494–1501.
- [30] H. Ishigaki, Laminar flow in rotating curved pipes, *J. Fluid Mech.* 329 (1996) 373–388.
- [31] H. Ishigaki, Laminar convective heat transfer in rotating curved pipes, *JSME Int. J. Ser. B* 42 (1999) 489–497.
- [32] G.T. Karahalios, Mixed convection flow in a heated curved pipe with core, *Phys. Fluid. A* 2 (12) (1990) 2164–2175.
- [33] M.A. Petrakis, G.T. Karahalios, Fluid flow behaviour in a curved annular conduit, *Int. J. Non-Linear Mech.* 34 (1999) 13–25.
- [34] G.T. Karahalios, Some possible effect of a catheter on the arterial wall, *Med. Phys.* 17 (1990) 922–928.
- [35] M.A. Ebadian, Rate of flow in a concentric pipe of circular cross-section, *J. Appl. Mech., Trans. ASME* 57 (1990).
- [36] G. Jayaraman, K. Tiwari, Flow in a catheterised curved artery, *Med. Biol. Eng. Comput.* 33 (5) (1995) 1–6.
- [37] R.K. Dash, G. Jayaraman, K.N. Mehta, Flow in a catheterised curved artery with stenosis, *J. Biomech.* 32 (1999) 49–61.
- [38] J.A. Chorin, Numerical solution of the Navier–Stokes equations, *Math. Comput.* 22 (104) (1968) 745–762.
- [39] W. Kays, M. Crawford, B. Weigand, *Convective Heat and Mass Transfer*, fourth ed. McGraw Hill, New York, 2005.